

PAPER • OPEN ACCESS

Numerical Study of Magnetohydrodynamic Blood Flow through an Artery with Multiple Stenosis

To cite this article: T Majekodunmi Joshua *et al* 2020 *IOP Conf. Ser.: Mater. Sci. Eng.* **864** 012199

View the [article online](#) for updates and enhancements.

You may also like

- [The effects of plaque morphological characteristics on the post-stenotic flow in left main coronary artery bifurcation](#)
Tahura Hossain, Noushin Anan and M Tarik Arafat
- [Non-isothermal flow of Sisko fluid in a stenotic tube induced via pulsatile pressure gradient and periodic body acceleration](#)
M Fahim, M Sajid and N Ali
- [Non-Newtonian pulsatile blood flow through the stenosed arteries: comparison between the viscoelastic and elastic arterial wall in response to the alterations](#)
Sahel Jannati, Mohammad Nabizadeh Shahri, Nahid Jafarzadeh *et al.*



ECS
The
Electrochemical
Society
Advancing solid state &
electrochemical science & technology

DISCOVER
how sustainability
intersects with
electrochemistry & solid
state science research

Numerical Study of Magnetohydrodynamic Blood Flow through an Artery with Multiple Stenosis

T Majekodunmi Joshua¹, K. Anwar¹ and N Abdullah¹

¹Institute of Engineering Mathematics, Universiti Malaysia Perlis, Malaysia

Email: majekjoe1@gmail.com

Abstract. The study theoretically accounts for the impact of Magnetohydrodynamics on streaming blood through an artery having multiple stenosis regions using the non-Newtonian Cross-rheological model. It is regarded that the streaming blood is unsteady and pulsative. The use of appropriate conditions is predicated on the assumption that the flow is laminar and axisymmetric which makes the problem two-dimensional. The geometry of stenosis was immobilized into a rectangular grid using the radial coordinate transformation. The finite difference scheme was employed for the numerical simulations. Specifically, magnetic field (Hartmann number), Reynolds number and severity of stenosis were varied over the entire arterial length. The results obtained predicted that increase in the Hartmann number and stenosis severity reduces the magnitude of the flow velocity, flow rate but the reverse is the case when the Reynolds number is increased. However, the wall shear stress and the resistance to flow are aided by increasing the Hartman number and the stenosis severity but reduces with increase in the Reynolds number. Hence, it is germane to apply the appropriate magnetic field in treatments otherwise, such patient may be vulnerable.

1. Introduction

The magnetohydrodynamic impact on free-flowing blood have recently been a crucial issue of examination among researcher owing to its indispensability in the treatment of diseases and its attending biological consequence. Magnetohydrodynamics (MHD) concerns itself with investigating the dynamics of electrically conducting fluids under the action of a magnetic field. Midya et al. [1] pointed out that blood can conduct electrical current as its obvious in real life.

The volume of blood oxygenation determines how susceptible it is to magnetism [2]. According to Saeed [2] and Vinay et al. [3], oxygenated blood exhibits a diamagnetic attribute of -6.67×10^{-7} and it usually flows from the heart to the arteries while blood manifest a paramagnetic attribute of 3.5×10^{-6} in its deoxygenated state as it flows through the veins to the heart. This suggest that MHD could probably influence blood flow within the cardiovascular system. As a result of the magnetic effect on the streaming blood, its charge particles are induced to rotate. Consequently, the suspension of erythrocyte increases in the plasma of the streaming blood which cumulates its internal viscosity. This rise in the blood viscosity generates a force otherwise known as the Lorentz force which serves as a resistance to the particles of the streaming blood. Hence, the blood velocity decreases in the magnetic field [4]. Over the years, MHD has gained a wide range of application which include MHD power generation, magnetic drug targeting during cancer treatment, MHD pumps, etc.

Studies have revealed that the flow field can be altered when a transverse magnetic-field is involved [5]. In order to examine the impact of MHD experimentally, Ichioka et al. [6] exposed some



rats to the magnetic field and observed a reduction in their temperature and blood flow rate. Hence, the import of MHD on blood flow cannot be undermined.

Majee and Shit [7] investigated the influence of MHD in the segment of a stenosed artery and observed that as the strength of the magnetic field (which largely depends on the Hartmann number) increases, certain parameters (both wall shear stress and the Nusselt number) of the flow field advances in magnitude and that such occurrence could be altered with the Reynolds number. They further explained that the wall of the artery won't be prone to injury until the magnetic field strength approaches 8T and that the resultant temperature variation could be used to treat diseases like hyperthermia. Similarly, a study on blood flow in a porous stenosed artery subjected to an external body acceleration with a uniform transverse magnetic-field by Das and Saha [8] revealed that when that Hartmann number is increased, the magnitude of the flow velocity and the volumetric flow rate declines. As a result, the wall shear stress is enhanced provided that the phase angle is kept constant. Their analysis seems to find its application in biomedical engineering.

The Cross model is a fluid model with four-parameters which best complies with the standardized viscosity shear-rate data of the human blood with hemoglobin 37% [9-10]. Its' uniqueness is that it illustrates the variation of effective viscosity within the entire shear rate range with more precision [11]. This model was employed by Achab et al. [12] in the numerical study of blood flow in a stenosed artery to capture some of the physical properties of blood viscosity at both medium and high shear rate. A comparison done by Shupti et al. [13] clearly reveals that among four (Carreau, Modified Casson, Cross and Quemada) models, only the Cross model is asymptotically equivalent to the constant viscosity at a shear rate greater than $100 s^{-1}$; which is most appropriate in non-Newtonian viscosity for blood flow [14].

The novelty of this study is that it accounts for the non-Newtonian attributes of streaming blood using the Cross model in an occluded artery that is characterized with multiple stenosis locations which conforms with the prevailing physiological assertions and can consequently be applicable in reality. The dynamic impact of MHD on the flow distribution of blood is also taken into consideration. The magnetic field intensity/ Hartmann number, severity of stenosis, Power Law index and the Reynolds number are varied in order to assess their individual impact on the flow velocity, flow rate, flow resistance and the wall shear stress.

2. Geometry of Stenosis

The geometry of the multiple stenosis is mathematically expressed in Equation 1;

$$R(z,t) = \begin{cases} a_1(t) \left[R_0 - \frac{\delta_1}{2} \left(1 + \cos \left(\frac{\pi(z-S_1)}{Z_1} \right) \right) \right], & S_1 - Z_1 < z < S_1 + Z_1 \\ a_1(t) \left[R_0 - \frac{\delta_2}{2} \left(1 + \cos \left(\frac{\pi(z-S_2)}{Z_2} \right) \right) \right], & S_2 - Z_2 < z < S_2 + Z_2 \\ a_1(t) [R_0], & \text{otherwise,} \end{cases} \quad (1)$$

where $R(z,t)$ and R_0 represents the arterial radius in both constricted and unconstricted portion respectively with a time variate parameter given in Equation 2;

$$a_1(t) = 1 + k_R \cos(\omega t - \phi) \quad (2)$$

where $\omega = 2\pi f_b$ stands for angular frequency and f_b is the pulse frequency with constant k_R . The profile of the geometry is described in Figure 1.

$$\frac{\partial w}{\partial t} + v \frac{\partial v}{\partial r} + w \frac{\partial w}{\partial z} = -\frac{1}{\rho} \frac{\partial p}{\partial z} \left[\frac{1}{r} \frac{\partial}{\partial r} (r \tau_{rz}) + \frac{\partial}{\partial z} (\tau_{zz}) \right] - \frac{\sigma B_0^2}{\rho} w, \quad (8)$$

$$\frac{\partial v}{\partial t} + v \frac{\partial v}{\partial r} + w \frac{\partial v}{\partial z} = -\frac{1}{\rho} \frac{\partial p}{\partial z} \left[\frac{1}{r} \frac{\partial}{\partial r} (r \tau_{rr}) + \frac{\partial}{\partial z} (\tau_{rz}) \right]. \quad (9)$$

The stress tensor component is of the form

$$\begin{aligned} \tau_{rr} &= -\mu \left(\dot{\gamma} \right) \left(2 \frac{\partial v}{\partial r} \right), & \tau_{zz} &= -\mu \left(\dot{\gamma} \right) \left(2 \frac{\partial w}{\partial z} \right), \\ \tau_{rz} = \tau_{zr} &= -\mu \left(\dot{\gamma} \right) \left(\frac{\partial v}{\partial z} + \frac{\partial w}{\partial r} \right), & \tau_{\theta\theta} &= -\mu \left(\dot{\gamma} \right) \left(2 \frac{v}{r} \right). \end{aligned}$$

The shear rate $\dot{\gamma}$ derived from the second invariant of the tensor is express in Equation 10;

$$\dot{\gamma} = \sqrt{2 \left[\left(\frac{\partial v}{\partial r} \right)^2 + \left(\frac{v}{r} \right)^2 + \left(\frac{\partial w}{\partial z} \right)^2 \right] + \left(\frac{\partial v}{\partial z} + \frac{\partial w}{\partial r} \right)^2} \quad (10)$$

The cross model was proposed by[8] as in Equation 11;

$$\mu \left(\dot{\gamma} \right) = \mu_{\infty} + (\mu_0 - \mu_{\infty}) \left[1 + \left(\frac{\dot{\gamma}}{\dot{\gamma}_c} \right)^m \right]^{-1}. \quad (11)$$

For an axisymmetric flow, the shear stress and shear rate are described in Equation 12, Equation 13 and Equation 14;

$$\tau_{zz} = -2 \left[\mu_{\infty} + (\mu_0 - \mu_{\infty}) \left\{ 1 + \dot{\gamma}_c^2 \left[2 \left(\left(\frac{\partial v}{\partial r} \right)^2 + \left(\frac{v}{r} \right)^2 + \left(\frac{\partial w}{\partial z} \right)^2 + \left(\frac{\partial v}{\partial z} + \frac{\partial w}{\partial r} \right)^2 \right] \right\}^{n-1/2} \right]^{-1} \cdot \left(\frac{\partial w}{\partial z} \right), \quad (12)$$

$$\tau_{rz} = - \left[\mu_{\infty} + (\mu_0 - \mu_{\infty}) \left\{ 1 + \dot{\gamma}_c^2 \left[2 \left(\left(\frac{\partial v}{\partial r} \right)^2 + \left(\frac{v}{r} \right)^2 + \left(\frac{\partial w}{\partial z} \right)^2 + \left(\frac{\partial v}{\partial z} + \frac{\partial w}{\partial r} \right)^2 \right] \right\}^{n-1/2} \right]^{-1} \cdot \left(\frac{\partial w}{\partial r} + \frac{\partial v}{\partial z} \right), \quad (13)$$

$$\tau_{rr} = -2 \left[\mu_{\infty} + (\mu_0 - \mu_{\infty}) \left\{ 1 + \dot{\gamma}_c^2 \left[2 \left(\left(\frac{\partial v}{\partial r} \right)^2 + \left(\frac{v}{r} \right)^2 + \left(\frac{\partial w}{\partial z} \right)^2 + \left(\frac{\partial v}{\partial z} + \frac{\partial w}{\partial r} \right)^2 \right] \right\}^{n-1/2} \right]^{-1} \cdot \left(\frac{\partial v}{\partial r} \right) \quad (14)$$

In Equation 7 to 14, V represents the radial velocity component while and W stand for the axial velocity components. ρ is the density of blood, the pressure is written as p and the stress tensor is denoted as τ . For non-Newtonian fluid, the dynamic viscosity is represented as $\mu \left(\dot{\gamma} \right)$.

The Cross model yields Newtonian values of μ_0 and μ_{∞} are very low and high shear rate [9] has described the pressure gradient as presented in Equation 15

$$-\frac{\partial p}{\partial z} = A_0 + A_1 \cos \omega t, \quad t > 0 \quad (15)$$

Here, the pressure gradient has an amplitude A_0 while A_1 stands for the amplitude of the unsteady part $w = 2\pi f$, f is the hearts' pulse frequency.

The streaming blood and arterial wall are related considering these initial and boundary conditions. In the axis, radial flow does not exist as well as the radial velocity and the velocity gradient [10].

$$v(r, z, t) = 0 \quad \frac{\partial w(r, z, t)}{\partial r} = 0 \quad \text{at } r = 0 \quad (16)$$

At a solid boundary, the velocity of blood will be equal to zero relative to the boundary. This is called 'the no-slip condition'.

$$w(r, z, t) = 0 \quad v(r, z, t) = 0 \quad \text{at } r = R \quad (17)$$

The initial velocity ($t = 0$) of flow is assumed to be Hagen-Poiseuille which describes its parabolic shape

$$w(r, z, 0) = \left(\frac{A_0 + A_1}{M^2} \right) \left\{ 1 - \frac{I_0(Mr)}{I_0(M)} \right\} v(r, z, t) = 0 \quad \text{for } M \neq 0 \quad (18a)$$

$$w(r, z, 0) = 2 \left(1 - \frac{r^2}{R^2} \right) v(r, z, t) = 0 \quad \text{for } M = 0 \quad (18b)$$

I_0 stands for the Bessel function of order zero. The boundary conditions are preserved by introducing arterial radii γ on the axial distance from both the onset and downstream of the constriction.

$$\text{Re} = \frac{\rho U R_0}{\mu}, \quad M^2 = \frac{B_0^2 \sigma R_0^2}{\mu} \quad (19)$$

Hence Equations 7 to 9 becomes as below (Equation 20, 21, and 22);

$$\frac{\partial v}{\partial r} + \frac{v}{r} + \frac{\partial w}{\partial z} = 0, \quad (20)$$

$$\frac{\partial w}{\partial t} + v \frac{\partial v}{\partial r} + w \frac{\partial w}{\partial z} = -\frac{1}{\rho} \frac{\partial p}{\partial z} \left[\frac{1}{r} \frac{\partial}{\partial r} (r \tau_{rz}) + \frac{\partial}{\partial z} (\tau_{zz}) \right] - \frac{M^2}{\text{Re}} w, \quad (21)$$

$$\frac{\partial v}{\partial t} + v \frac{\partial v}{\partial r} + w \frac{\partial v}{\partial z} = -\frac{1}{\rho} \frac{\partial p}{\partial z} \left[\frac{1}{r} \frac{\partial}{\partial r} (r \tau_{rr}) + \frac{\partial}{\partial z} (\tau_{rz}) \right]. \quad (22)$$

3.2. Solution Procedure

The radial co-ordinate transformation expressed in Equation 23

$$\xi = \frac{r}{R_{(z,t)}} \quad (23)$$

is used to immobilize the vessel wall in the newly transformed coordinate ξ , the continuity Equation 20 becomes (Equation 24);

$$\frac{1}{R} \frac{\partial v}{\partial \xi} + \frac{v}{\xi R} + \frac{\partial w}{\partial z} - \frac{\xi}{R} \frac{\partial w}{\partial \xi} \frac{\partial R}{\partial z} = 0. \quad (24)$$

The axial momentum in Equation 21 becomes (Equation 25);

$$\begin{aligned} \frac{\partial w}{\partial t} = & \left[\frac{\xi}{R} \cdot \frac{\partial R}{\partial t} - \frac{v}{R} + w \frac{\xi}{R} \cdot \frac{\partial R}{\partial z} \right] \frac{\partial w}{\partial \xi} - w \frac{\partial w}{\partial z} - \frac{1}{\rho} \frac{\partial p}{\partial z} \\ & - \frac{1}{\rho} \left[\frac{1}{\xi R} \tau_{\xi z} + \frac{1}{R} \frac{\partial \tau_{\xi z}}{\partial x} + \frac{\partial \tau_{zz}}{\partial z} - \frac{\xi}{R} \frac{\partial \tau_{zz}}{\partial \xi} \frac{\partial R}{\partial z} \right] - \frac{M^2}{\text{Re}} w. \end{aligned} \quad (25)$$

The normal stress τ_{zz} in equation (12) also becomes (Equation 26);

$$\begin{aligned} \tau_{zz} = & -2 \left[\mu_{\infty} + (\mu_0 - \mu_{\infty}) \left\{ 1 + \gamma_c^2 \left[2 \left(\left(\frac{1}{R} \cdot \frac{\partial v}{\partial r} \right)^2 + \left(\frac{v}{\xi R} \right)^2 \right. \right. \right. \right. \\ & + \left. \left. \left(\frac{\partial w}{\partial z} - \frac{\xi}{R} \cdot \frac{\partial R}{\partial z} \cdot \frac{\partial w}{\partial \xi} \right)^2 + \left(\frac{\partial v}{\partial z} - \frac{\xi}{R} \cdot \frac{\partial R}{\partial z} \cdot \frac{\partial v}{\partial \xi} \right. \right. \right. \\ & \left. \left. \left. + \frac{1}{R} \cdot \frac{\partial w}{\partial \xi} \right)^2 \right\}^{\frac{n-1}{2}} \right]^{-1} \times \left(\frac{\partial w}{\partial z} - \frac{\xi}{R} \frac{\partial R}{\partial z} \frac{\partial w}{\partial \xi} \right). \end{aligned} \quad (26)$$

Similarly, the shear stress in equation (13) becomes (Equation 27);

$$\begin{aligned} \tau_{\xi z} = & - \left[\mu_{\infty} + (\mu_0 - \mu_{\infty}) \left\{ 1 + \gamma_c^2 \left[2 \left(\left(\frac{1}{R} \cdot \frac{\partial v}{\partial r} \right)^2 + \left(\frac{v}{\xi R} \right)^2 \right. \right. \right. \right. \\ & + \left. \left. \left(\frac{\partial w}{\partial z} - \frac{\xi}{R} \cdot \frac{\partial R}{\partial z} \cdot \frac{\partial w}{\partial \xi} \right)^2 + \left(\frac{\partial v}{\partial z} - \frac{\xi}{R} \cdot \frac{\partial R}{\partial z} \cdot \frac{\partial v}{\partial \xi} \right. \right. \right. \\ & \left. \left. \left. + \frac{1}{R} \cdot \frac{\partial w}{\partial \xi} \right)^2 \right\}^{\frac{n-1}{2}} \right]^{-1} \times \left(\frac{1}{R} \frac{\partial w}{\partial \xi} + \frac{\partial v}{\partial z} - \frac{\xi}{R} \frac{\partial R}{\partial z} \frac{\partial v}{\partial \xi} \right). \end{aligned} \quad (27)$$

The boundary conditions Equation 16 to 18b) using the radial transformation becomes as below (Equation 28 to 30b);

$$v(\xi, z, t) = 0, \quad \frac{\partial w(\xi, z, t)}{\partial r} = 0, \quad \tau_{\xi z} = 0 \quad \text{on} \quad \xi = 0 \quad (28)$$

$$v(\xi, z, t) = \frac{\partial R}{\partial t}, \quad w(\xi, z, t) = 0 \quad \text{on} \quad \xi = 1, \quad (29)$$

$$w(\xi, z, 0) = \left(\frac{A_0 + A_1}{M^2} \right) \left\{ 1 - \frac{I_0(M\xi R)}{I_0(M)} \right\}, \quad (30a)$$

$$\text{Also } v(\xi, z, 0) = 2(1 - \xi^2). \quad (30b)$$

The components $v(\xi, z, t)$ of the radial velocity is deduced by multiplying the transformed equation of continuity Equation (24) by ξR then integrate with respect to ξ from limit 0 to limit ξ i.e. from $\xi \rightarrow 0$.

$$\int_0^\xi \xi \frac{\partial v}{\partial \xi} d\xi + \int_0^\xi v d\xi + \int_0^\xi \xi R \frac{\partial w}{\partial z} d\xi - \int_0^\xi \xi^2 \frac{\partial w}{\partial \xi} \frac{\partial R}{\partial z} d\xi = 0,$$

$$\xi v - \int_0^\xi v d\xi + \int_0^\xi v d\xi + R \int_0^\xi \xi \frac{\partial w}{\partial z} d\xi - \frac{\partial R}{\partial z} \left[\int_0^\xi \xi^2 w d\xi - \int_0^\xi 2\xi w d\xi \right] = 0.$$

When simplified, it yields

$$\xi v + R \int_0^\xi \xi \frac{\partial w}{\partial z} d\xi - \frac{\partial R}{\partial z} \xi^2 w + \frac{\partial R}{\partial z} \int_0^\xi 2\xi w d\xi = 0,$$

$$v(\xi, z, t) = \xi \frac{\partial R}{\partial z} w - \frac{R}{\xi} \int_0^\xi \xi \frac{\partial w}{\partial z} d\xi - \frac{2}{\xi} \frac{\partial R}{\partial z} \int_0^\xi \xi w d\xi. \quad (31)$$

Applying the boundary condition in Equation 28 to Equation 30b gives

$$-\int_0^1 \xi \frac{\partial w}{\partial z} d\xi = \int_0^1 \xi \left[\frac{2}{R} \frac{\partial R}{\partial z} w + \frac{1}{R} \frac{\partial R}{\partial t} f(\xi) \right] d\xi. \quad (32)$$

$f(\xi)$ is arbitrarily chosen

$$f(\xi) = 4(1 - \xi^2) \text{ which satisfies } \int_0^1 \xi f(\xi) d\xi = 1. \quad (33)$$

Compare the left hand side of the arbitrary function to equation

$$\frac{\partial w}{\partial z} = -\frac{2}{R} \frac{\partial R}{\partial z} w + \frac{4}{R} (\xi^2 - 1) \frac{\partial R}{\partial t}. \quad (34)$$

Substituting Equation 33 into 31, we obtain

$$v(\xi, z, t) = \xi \left[\frac{\partial R}{\partial z} w + \frac{\partial R}{\partial t} (2 - \xi^2) \right]. \quad (35)$$

3.3. Discretization using finite difference scheme

The central difference approximation is employed in finite difference scheme to solve Equation 24 and 25 for all the first spatial derivatives which are:

$$\frac{\partial w}{\partial z} = \frac{(w)_{i+1,j}^k - (w)_{i-1,j}^k}{2\Delta z} = w_{fz}, \quad \frac{\partial w}{\partial \xi} = \frac{(w)_{i,j+1}^k - (w)_{i,j-1}^k}{2\Delta \xi} = w_{f\xi}. \quad (36)$$

For the time derivative Equation 21, consider

$$\frac{\partial w}{\partial t} = \frac{(w)_{i,j}^k - (w)_{i,j}^{k-1}}{\Delta t}. \quad (37)$$

$w(\xi, z, t)$ is written as $w(\xi_j, z_i, t_k)$ for the purpose of discretization and hence denoted by $w_{i,j}^k$. Parameters are therefore defined as:

$$\xi_j = (j-1)\Delta\xi; \quad j = 1, 2, \dots, N+1 \quad x_{N+1} = 1.0$$

$$z_i = (i-1)\Delta z; \quad i = 1, 2, \dots, M+1,$$

$$t_k = (k-1)\Delta t; \quad k = 1, 2, \dots$$

By substituting equations (35)- (36) appropriately, the discretized form of Equations 25, 26 and 27 are

$$\begin{aligned} (w)_{i,j}^{k+1} = & (w)_{i,j}^k + \Delta t \left[\frac{\xi_j}{R_i^k} \left(\frac{\partial R}{\partial t} \right)_i^k - \frac{v_{i,j}^k}{R_i^k} + (w)_{i,j}^k \cdot \frac{\xi_j}{R_i^k} \left(\frac{\partial R}{\partial z} \right)_i^k \right] \left(\frac{\partial w}{\partial \xi} \right)_{i,j}^k - w_{i,j}^k \cdot (w_{fz})_{i,j}^k - \frac{1}{\rho} \left(\frac{\partial p}{\partial z} \right)_i^{k+1} \\ & - \frac{1}{\rho} \left[\frac{1}{\xi_j R_i^k} \tau_{\xi z} + \frac{1}{R_i^k} \left[(\tau_{\xi z})_{f\xi} \right]_{i,j}^k + \left[(\tau_{zz})_{fz} \right]_{i,j}^k - \frac{\xi_j}{R_i^k} \left[(\tau_{zz})_{\xi} \right]_{i,j}^k \left(\frac{\partial R}{\partial z} \right)_i^k \right] - \frac{M^2}{\text{Re}} w, \end{aligned} \quad (38)$$

$$\begin{aligned} \tau_{zz} = & -2 \left[\mu_{\infty} + (\mu_0 - \mu_{\infty}) \left\{ 1 + \gamma_c^2 \left[2 \left(\left(\frac{1}{R_i^k} \cdot (v_{fz})_{i,j}^k \right)^2 + \left(\frac{(v)_{i,j}^k}{\xi_j R_i^k} \right)^2 + \left((w_{fz})_{i,j}^k - \frac{\xi_j}{R_i^k} \cdot \left(\frac{\partial R}{\partial z} \right)_i^k \cdot (w_{f\xi})_{i,j}^k \right)^2 \right] \right\} \right. \\ & \left. + \left((v_{fz})_{i,j}^k - \frac{\xi_j}{R_i^k} \cdot \left(\frac{\partial R}{\partial z} \right)_i^k \cdot (v_{f\xi})_{i,j}^k + \frac{1}{R_i^k} \cdot (w_{f\xi})_{i,j}^k \right)^2 \right]^{\frac{n-1}{2}} \times \left((w_{fz})_{i,j}^k - \frac{\xi_j}{R_i^k} \left(\frac{\partial R}{\partial z} \right)_i^k (w_{f\xi})_{i,j}^k \right), \end{aligned} \quad (39)$$

$$\tau_{\xi z} = -[\dots]^{-1} \times \left((v_{fz})_{i,j}^k - \frac{\xi_j}{R_i^k} \left(\frac{\partial R}{\partial z} \right)_i^k \cdot (v_{f\xi})_{i,j}^k + \frac{1}{R_i^k} (w_{f\xi})_{i,j}^k \right). \quad (40)$$

The discretised boundary conditions (Equation 28-30b) is of the form

$$(v)_{i,j}^k = 0, \quad (w)_{i,1}^k = (w)_{i,2}^k \quad (\tau_{\xi z})_{i,1}^k = 0, \quad (41)$$

$$(w)_{i,N+1}^k = 0, \quad (v)_{i,N+1}^k = \left(\frac{\partial R}{\partial t} \right)_i^k, \quad (42)$$

and

$$(v)_{i,j}^1 = 0, \quad (w)_{i,j}^1 = 0. \quad (43)$$

Equation (34) is discretized as

$$(v)_{i,j}^{k+1} = \xi_j \left[\left(\frac{\partial R}{\partial z} \right)_i^k w_{i,j}^{k+1} + \left(\frac{\partial R}{\partial t} \right)_i^k (2 - \xi_j^2) \right]. \quad (44)$$

The flow rate (Q), resistance to flow (v), as well as the shear-stress on the wall (τ_w) are mathematically expressed as [18]:

$$Q_i^k = 2\pi (R_i^k)^2 \int_0^1 \xi (w)_{i,j}^k d\xi_j, \quad (45)$$

$$v_i^k = \frac{|L(\partial p / \partial z)^k|}{Q_i^k}, \quad (46)$$

$$(\tau_w)_i^k = \mu \left[\frac{1}{R_i^k} \cdot (w_{f\xi})_{i,j}^k + (v_{fz})_{i,j}^k - \frac{\xi_j}{R_i^k} (v_{f\xi})_{i,j}^k \cdot \frac{\partial R^k}{\partial z_i} \right]_{\xi=1} \times \cos \left(\tan^{-1} \left(\frac{\partial R}{\partial z} \right)_i \right). \quad (47)$$

4. Discussion and Results

The characteristics of the flow field are expressed with regard to the axial velocity, flow rate, resistance to flow and the wall shear stress distribution for varying values of the Hartmann number (M), Reynolds number (Re), the power law index (n) as well as the severity of Stenosis (δ) with which the blood flow responses under these changes are measured. As suggested by [19-20], the numerical simulations were performed with following parameter values:

$\delta_1 = \delta_2 = 0.276R_0$, $Re = 300$, $\rho = 1.06 \text{ gcm}^{-3}$, $k_r = 0.0001$, $a = 0.154 \text{ cm}$, $\phi = 0^\circ$,
 $\Delta x = 0.025$, $f_b = 1.2 \text{ Hz}$ with time step $\Delta t = 0.0001$, convergence is attained with an accuracy of order $\times 10^6$. Solutions are computed for this computational domain using the grid 60×40 for z and x respectively.

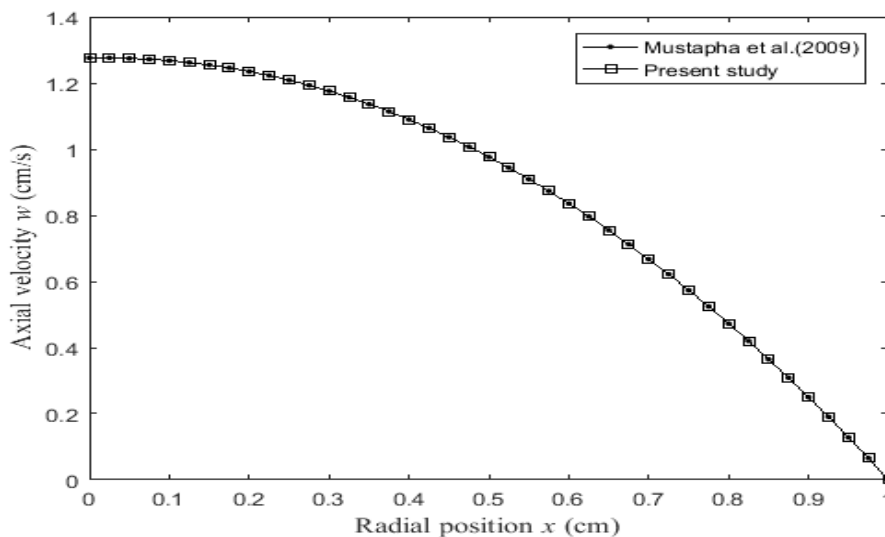


Figure 2. Axial velocity of a multiple stenosed artery at $M = 0$

As shown in Figure 2, a good agreement is observed in the comparison made at $M = 0$ for the axial velocity distribution of the streaming blood between the present study and those of Mustapha et al. [20] who examined a Newtonian MHD blood flow, for the purpose of validity.

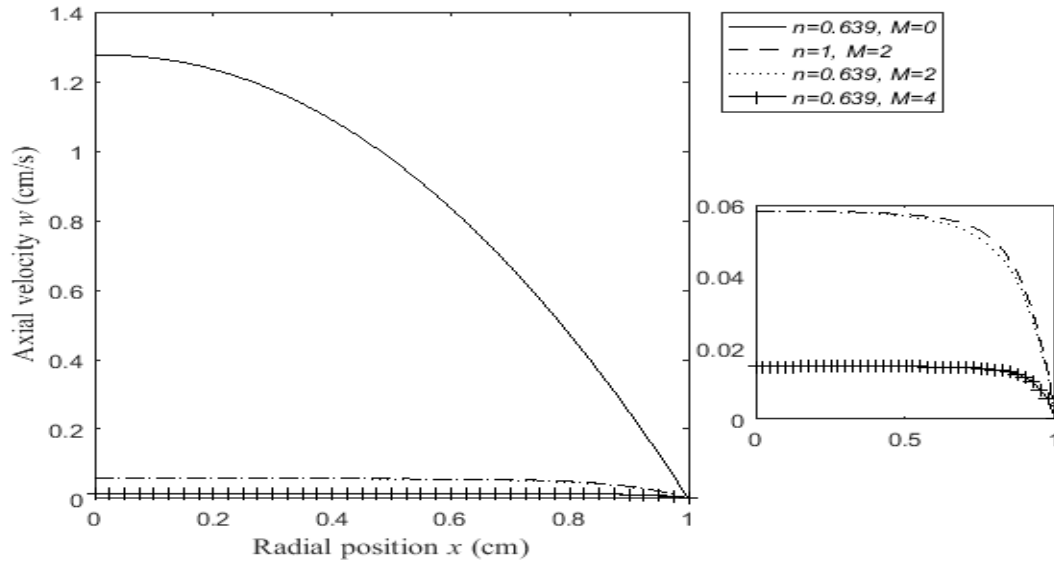


Figure 3. Axial velocity profile distribution at different Hartmann number

Figure 3 illustrates the axial velocity distribution for certain values of the Hartmann number. From the present figure, the axial velocity decrease as the Hartmann number (variable of the magnetic field) increases. This have a close similarity with those of Abdullah et al. [21] and Mustapha et al. [20]. As the magnitude of the Hartmann number increases, the axial velocity curves tend toward the origin. This observation is similar to those of Srivastava [22] who investigated the influence of the magnetic field on an inclined tapered artery in a porous media. The Newtonian assumption seem to predict the same magnitude of axial velocity as the Cross model at a constant Hartmann number $M = 2$. Based on this result, we can conclude that the magnetic parameter greatly influences the axial velocity of the streaming blood more than the non-Newtonian model.

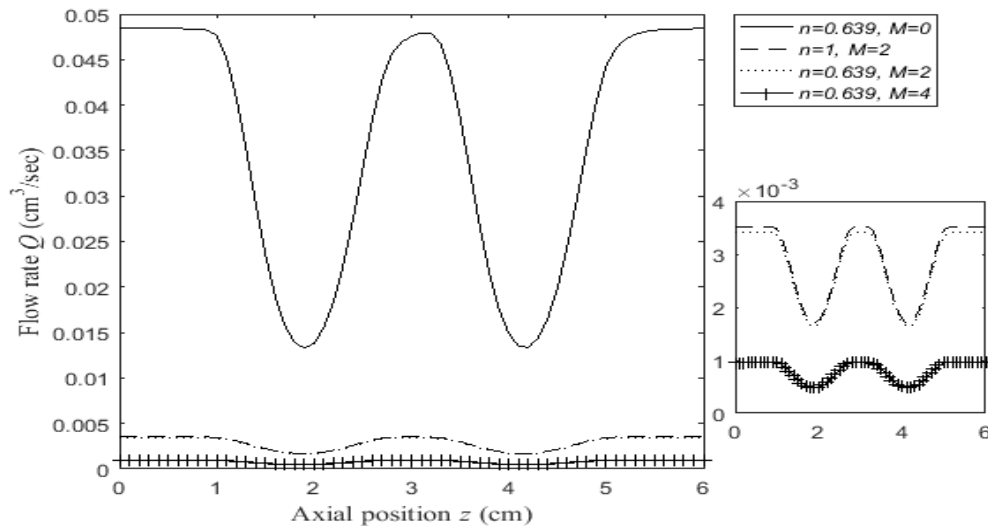


Figure 4. Flow rate distribution at different Hartmann number

Figure 4 depicts the distribution in the flow rate over the whole arterial length for varying magnitude of Hartmann number M and the Newtonian assumption. From this present figure, the flow rate decreases with heightening values of the Hartmann number (M). This seem to be in good harmony with Srivastava [22], Sharma et al. [5], Abdullah et al. [21] who studied the effect of the magnetic field on flow parameters though their work was based on single stenosis. Notwithstanding, if the Hartmann number is kept constant at $M = 2$ and the Newtonian model is assumed, only a meagre decline is observed in the flow rate: indicating that the magnetic parameter/ Hartmann number influences the rate of the flowing blood more than the non-Newtonian rheology. We can draw an inference when the present figure is compared with figure 2 that the Hartmann number exerts similar influence on both axial velocity of blood as well as its flow rate.

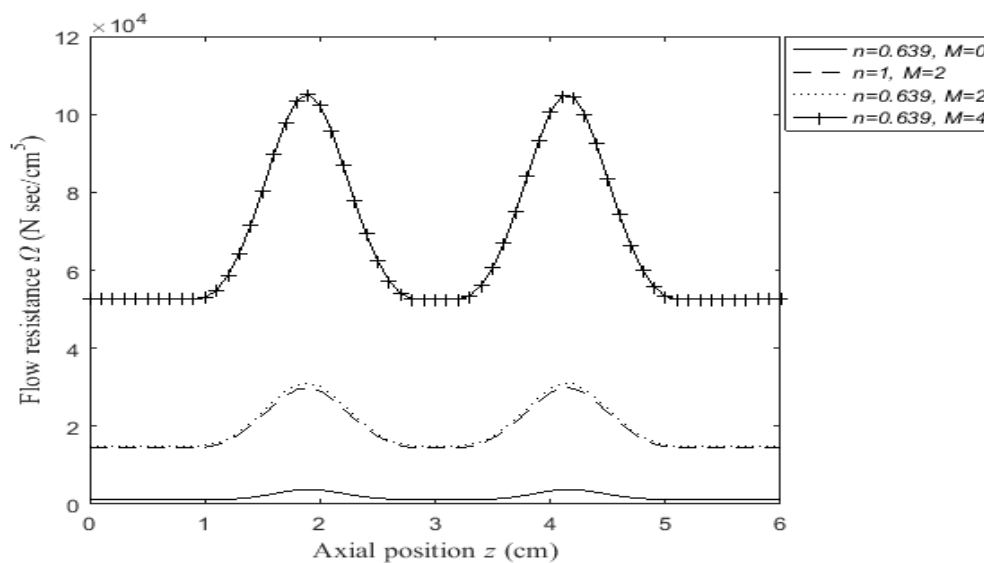


Figure 5. Flow resistance distribution at different Hartmann number

Figure 5 depicts the profile of the flow resistance for the entire arterial length at certain value of the Hartmann number with a Newtonian assumption at time $t=0.50s$. Unlike both axial velocity and flow rate in figure 2 and figure 3, each increment in the Hartmann number M led to an increase in the flow impedance /resistance with uniform peaks at specific locations of the arterial maximum constriction. This conforms with the finding of Abbas et al.[23] and Ponalagusamy & Priyadharshini [24]. Furthermore, Ponalagusamy & Priyadharshini [24] opined that the rate at which blood flows is significantly reduced when the magnetic effect is considered in blood flow. Though, the Newtonian assumption, when the value of the Hartmann number is kept constant at $M = 2$ seem to predict a slightly higher value of the the flow resistance from the present figure, it is obvious that its effect is meager as compared to those of the magnetic parameter.

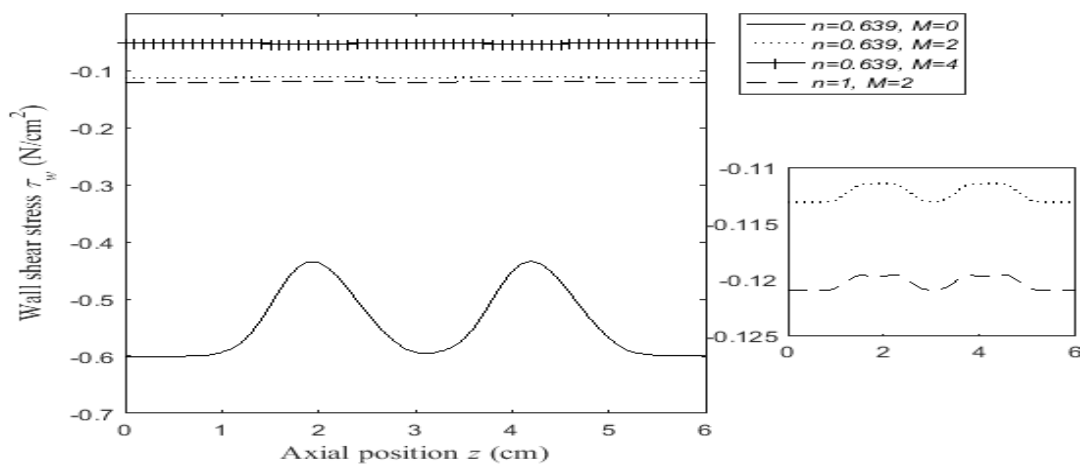


Figure 6. Wall shear stress distribution at different Hartmann number

Figure 6 portrays the walls shear stress profile for varied magnitudes of Hartmann number of the magnetic field across the segment of the artery at Reynold number $Re=300$. A similar trend and pattern is observed for the curves which is notable at the crest /most constricted region. Also, an increase in the Hartmann number led to a proportionate increase in the wall shear stress (which indicate an opposite trend to those of the axial velocity as well as the flow rate as seen in figure 2 and figure 3 respectively) with no possibility of backflow or zone of separation. This result agrees well with those of Midya et al. [1], Ponalagusamy & Priyadharshini [24], Mustapha et al. [20] and Abdullah et al. [21]. However, a slight increase was observed in the magnitude of the wall shear stress when the Newtonian assumption was taken into consideration which is in conformity with Ikbal et al. [25].

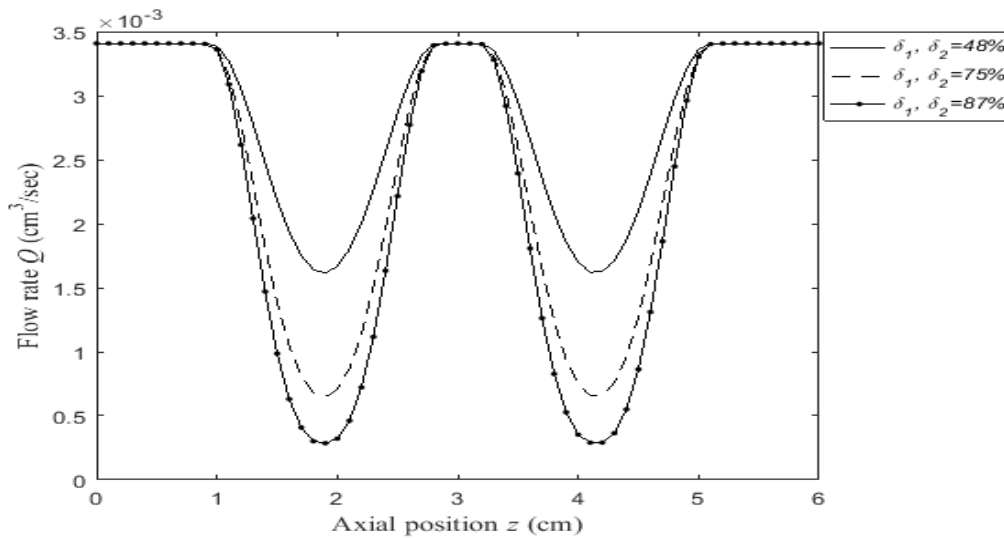


Figure 7. Flow rate distribution at different stenosis severity

Figure 7 illustrates the axial variation in the flow rate of the streaming blood for specific occlusion or severity values at a constant Hartmann number. As expected, the flow rate of blood reduces and the the severity or height of stenosis is increased. This substantiate the observation of Shaw et al. [26] who studied the influence of periodic body acceleration with magnetohydrodynamics on blood flow through an asymmetric stenosis using the Casson model. The flow rate seem to be steady at the unobstructed portion (onset) and thereafter declines drastically until its maximum constriction. This is accompanied by a rise towards the stenosis downstream and a similar trend is repeated for then second stenosis.

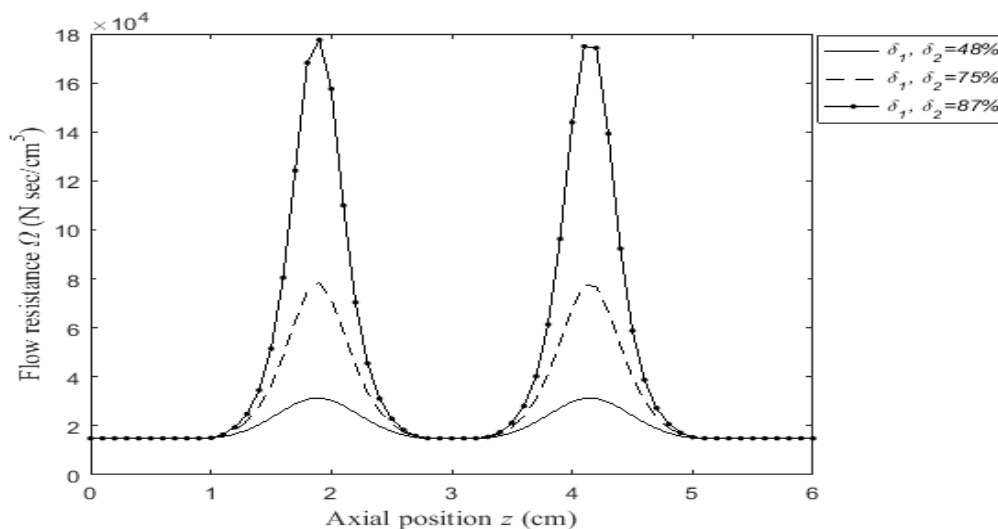


Figure 8. Flow resistance distribution at different stenosis severity.

The resistance to flow at different stenosis severity at a constant Hartmann number $M = 2$ is depicted in Figure 8. It's quite obvious from the deduced curves that the flow resistance increases with respect to the worsening severity of the stenosis. i.e. increase in the severity leads to a rise in the flow resistance. This is also in line with the observation made by Shaw et al. [27]. Notably, all curves follow a similar pattern with prominent peaks at a specific location.

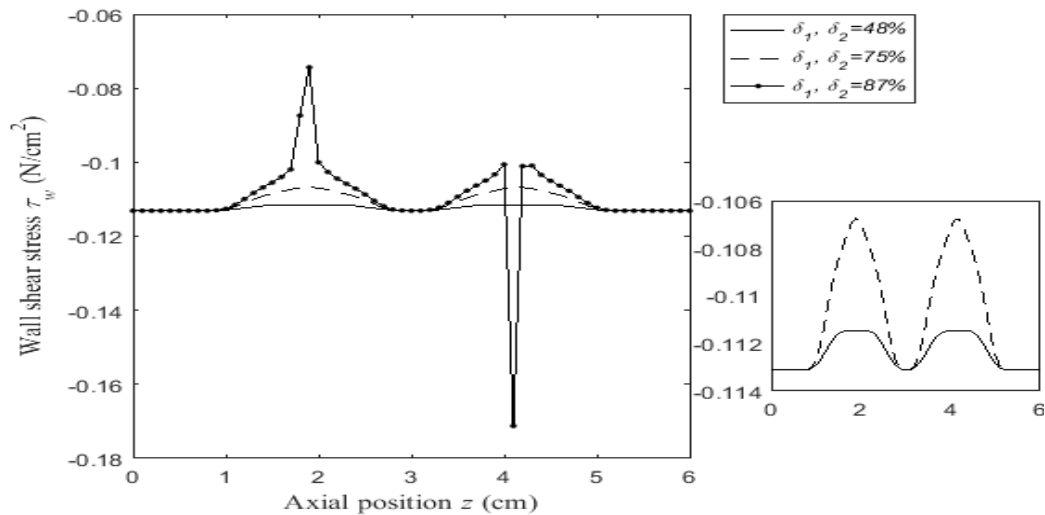


Figure 9. Wall shear stress distribution at different stenosis severity

Figure 9 outlines the axial distribution of the wall shear stress. From the figure, the wall shear stress appears to be directly proportional to the severity of the stenosis. i.e. increase in the severity initiates an increase in the magnitude of the wall shear stress which is uniform with the observation of Priyadharshini and Ponalagusamy [24-27]. Regular peaks of the wall shear stress showing their maximum contractions are observed at specific locations especially at 48% and 75% occlusion. However, at 96% severity/ blockage, the wall shear stress assumes its least value on the trough formed after the maximum constriction and thereafter rises to the peak for the first stenosis. Almost the same trend was repeated at the onset of the second stenosis but a crest was formed after its initial rise crossing its separation zone. This peculiarity may be due to its height of severity.

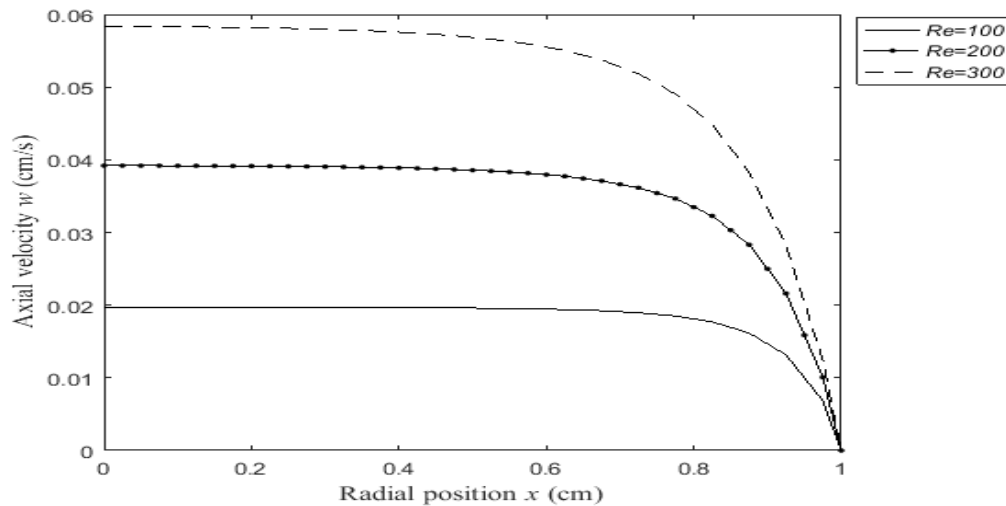


Figure 10. Axial velocity distribution at different Reynolds number

Figure 10 depicts the impact of the Reynolds number on the axial velocity at constant Hartmann number $M = 2$. It was observed that the Reynolds number increases proportionately as the axial velocity with similar curve pattern. An increase in the Reynolds number reduces the viscous force that resists relative motion within the layers of the streaming blood. Hence, the free flow of blood is enhanced and the magnitude of the axial velocity consequently rises. This corroborate with the findings of Majee and Shit [7] and Mwangi [28]. Comparing the present figure with the figure 2 clearly reveals that the magnitudes of both the Hartmann number and the Reynold number influence the axial velocity significantly.

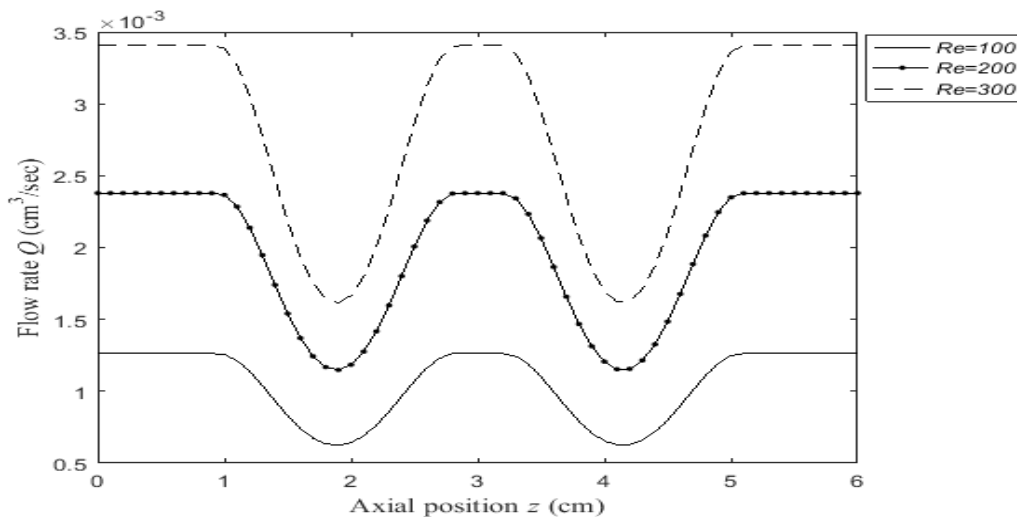


Figure 11. Flow rate distribution at different Reynolds number

Figure 11 illustrates the distribution of the flow rate for different Reynolds number while the Hartmann number is kept constant at $M = 2$. Obviously, from the curves in the present graph, increasing the Reynolds number enhances the blood flow rate. This is in line with the result obtained by Sharma et al. [5] who investigated the slip effect on an inclined catheterized stenosed arterial wall. The flow rates were higher at the non-stenosed portion followed by a sharp decline toward the region with maximum constriction and subsequently rise as it approaches the stenosis downstream. A similar sequence is observed at the second stenosis.

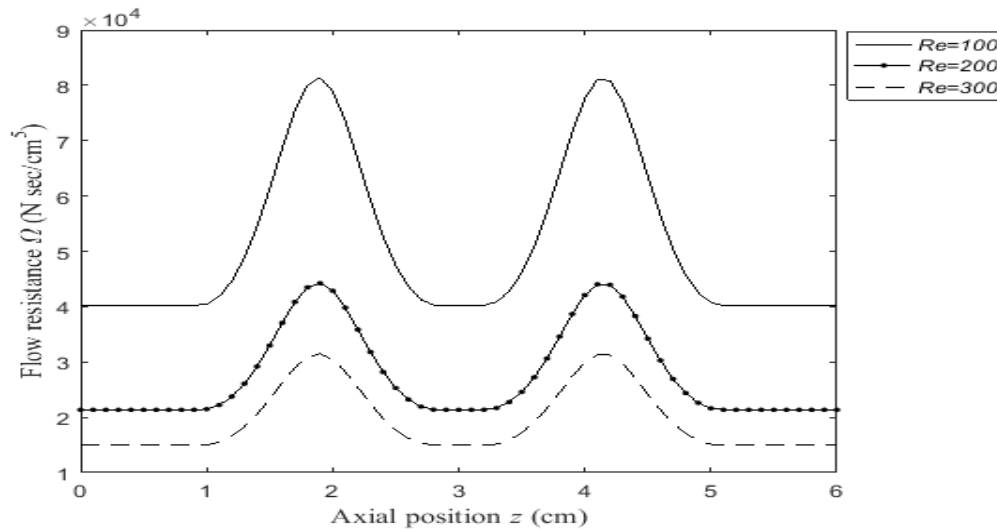


Figure 12. Flow resistance distribution at different Reynolds number

The distribution of the flow resistance with the axial distance for specific values of the Reynolds number ($Re = 300$) at constant Hartmann number ($M = 2$) is depicted in Figure 12. The flow resistance reduces with increase in the Reynolds number. This reflect the inverse relationship between both parameters which corroborates with the findings of Ponalagusamy and Priyadharshini [27] though their study assumed a tapered arterial stenosis in a porous media.

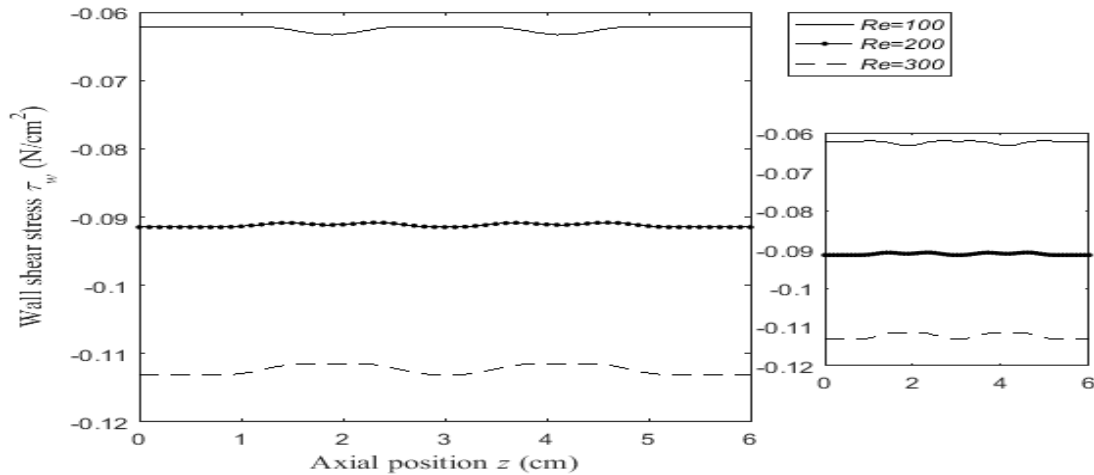


Figure 13. Wall shear stress distribution at different Reynolds number

Figure 13 describes the variation in the wall shear stress (τ_w) with respect to the axial distance for different Reynolds number at a constant Hartmann number $M = 2$. As the Reynolds number increases, the magnitude of the wall shear stress reduces, having a regular curve pattern with notable peaks at the maximum constriction. This observation is in accordance with the inference of Sharma et al. [5].

5. Conclusion

The unsteady blood flow through a multiple inclined stenosis under the influence of the magnetic field has been examined in this study. The pathogenesis of atherosclerosis has been taken into consideration; by noting the magnitude of severity ($\delta = 48\%$, 75% , 96%). The results of the numerical simulation have been presented for the flow field which include the axial velocity, flow rate, resistance to flow and the wall shear stress using the Finite-Difference Scheme. From the analysis of the obtained result, the following inferences are deduced:

- i. Increase of the Hartmann number (variable of the magnetic field) reduces the flow velocity. On the other hand, the axial velocity is heightened by increasing the Reynolds number. This is because, the Reynolds number reduces the viscous force within the layers of the fluid (streaming blood) thereby aiding its free flow.
- ii. The magnetic parameter greatly influences the axial velocity of the streaming blood while the non-Newtonian model contributes a less significant effect.
- iii. As both Hartmann number and the severity of stenosis increases, the flow rate of blood reduces. However, increasing magnitude of the Reynolds number strengthens the flow rate.

Both flow resistance and the wall shear stress are aided by increasing the Hartmann number and the stenosis severity but reduces with increase in the Reynolds number.

References

- [1] Midya C, Layek G C, Gupta A S, and Mahapatra T R 2003 *J. Fluids Eng.* **125** 952-962
- [2] Saeed A B 2017 *PhD Thesis Universiti Teknologi Malaysia* 2017
- [3] Vinay M. Pai C J C and Yousef Haik 1996 *Fluid Dyn. interfaces, Cambridge University Press, Cambridge* 439-452
- [4] Tripathi B and Sharma B K 2018 *Int. J. Appl. Mech. Eng.* **23(3)** 767-785
- [5] Sharma M K, Singh K and Bansal S 2014 *J. Biomed. Sci. Eng.* **07** 194-207

- [6] Ichioka S 2000 *The European Bioelectromagnetics Association* **21** 183-188
- [7] Majee S and Shit G C 2017 *J. Magn. Magn. Mater.* **424** 137–147
- [8] Das G C and Kalidas Saha 2009 *Math. Subj. Classif.* **16** 21-42
- [9] Akbar Zaman N K and Mazhar Sajjad 2018 *Canadian Journal of Physics* **97** 487-497
- [10] Hutton J F, Walters K and Barnes H A 1989 *An Introduction to Rheology, Elsevier, Amsterdam*
- [11] Tazyukov F K, Khalaf H A and Hassan J M 2011 *International Mechanical Engineering Congress and Exposition, Colorado-USA*
- [12] Achab L, Mahfoud M and Benhadid S 2016 *Therm. Sci.* **20** 449–460
- [13] Shupti S P, Rabby M G and Molla M 2015 *Journal of Fluids*
- [14] Azahari A, Ismail Z and Abdullah N 2018 *Matematika* **34** 87–102
- [15] Cross M M 1965 *J. Colloid Sci.* **20** 417–437
- [16] Burton A C 1966 *Physiology and biophysics of the circulation : an introductory text TT Year Book Medical Publishers, Chicago, Ill*
- [17] Bin Tan Y and Mustapha N 2016 The Gravitational Effects of Blood Flow in Irregular Stenosed Artery with Various Severity Problem Formulation **2** 28–39
- [18] Mandal P K 2015 *Int. J. Non. Linear. Mech.* **40** 151–164
- [19] McDonald D A 1974 *McDonald's blood flow in arteries: theoretical, experimental and clinical principles, 1st edition. Edward Arnold*
- [20] Mustapha N, Amin N, Chakravarty S and Mandal P. K 2009 *Comput. Biol. Med.* **39** 896–906
- [21] Abdullah I, Amin N and Hayat T 2010 *Int. J. Numer. Methods Fluids* **67** 1624–1636
- [22] Srivastava N 2014 *J. Biophys.* **2014** 797142
- [23] Abbas Z, Shabbir M S and Ali N 2018 *Results Phys.* **9** 753–762
- [24] Priyadharshini S and Ponalagusamy R 2017 *Sadhana - Acad. Proc. Eng. Sci.* **42** 1901–1913
- [25] Ikbal M A, Chakravarty S, Wong K K L, Mazumdar J and Mandal P K 2009 *J. Comput. Appl. Math.* **230** 243–259
- [26] Shaw S, Murthy P V S N and Pradhan S C 2010 *Open Transp. Phenom. J.* **2** 55–68
- [27] Ponalagusamy R and Priyadharshini S 2017 *J. Mech. Med. Biol.* **17(8)** 1750109
- [28] Mwangi K J 2016 *Unsteady magnetohydrodynamic fluid flow in a collapsible tube* (Doctoral dissertation, Applied Mathematics, JKUAT)